Phase formation in ion-irradiated and annealed Ni-rich Ni-Al thin films

Dale E. Alexander[a] and Gary S. Was
Department of Nuclear Engineering, University of Michigan, Ann Arbor, Michigan 48109

L. E. Rehn
Argonne National Laboratory, 9700 South Cass Avenue, Argonne, Illinois 60439

(Received August 24, 1990; accepted for publication 2 November 1990)

Phase formation was studied in ion-irradiated multilayer and coevaporated Ni-20 at. % Al films supported by Cu, Mo, and Ni transmission electron microscopy (TEM) grids. Irradiation with either 700-keV Xe or 1.7-MeV Xe, to doses sufficient to homogenize the multilayers ($\geqslant 7.5\times 10^{15}$ cm^{-2}), resulted in the formation of metastable supersaturated γ and HCP phases in both film types. Post-irradiation annealing of multilayers at 450 °C for 1 h transformed the metastable phases to a two-phase $\gamma+\gamma'$ microstructure. In the absence of Cu, the formation of γ' appeared to proceed by a traditional diffusional growth mechanism, resulting in small (<50 Å) γ' precipitates in γ matrix grains. The presence of Cu caused the formation of a dual-phase $\gamma+\gamma'$ structure (i.e., distinct, equal-sized grains of γ and γ') during post-irradiation annealing. It is suggested that copper affected the nucleation of γ' precipitates and increased the kinetics of growth resulting in the dual-phase morphology. Strong irradiation-induced textures were observed in the multilayers that were less pronounced in the coevaporated films. The texture in the multilayers was attributed to the presence of a slight as-evaporated texture combined with the enhanced atomic mobility due to the heat-of-mixing released during irradiation. The irradiation-induced texture appeared to be necessary for the formation of the dual-phase structure since it likely provided high-diffusivity paths for Cu to diffuse into the film from the TEM grid.

I. INTRODUCTION

The use of ion beams for the production of metastable phases in metal alloy thin films and surfaces has been the subject of considerable study in the past decade. The binary Ni-Al alloy system has been the focus of a number of such studies[1-13] because of its technological importance. This system forms the basis of many of the so-called superalloys commonly used in high-temperature and strength applications.[14] As a result, considerable effort has been devoted in the last 40 years to characterizing the thermodynamics, reaction kinetics, and microstructures in the Ni-Al system. Ion-beam studies using Ni-Al therefore benefit from a comprehensive database upon which to interpret irradiation-induced phase formation results. Additionally, the unique structures often produced by ion irradiation offer potential benefits such as improvement of surface-related mechanical properties.[13]

Figure 1 shows the equilibrium phase diagram for the Ni-Al system.[15] In the Ni-rich end two phases are present, the gamma phase (γ) and the gamma-prime phase (γ'). The γ phase is a FCC Ni lattice with Al occupying substitutional sites in the composition range of 0–7 at. % Al ($T\leqslant 400$ °C).[15] The γ' phase is an ordered intermetallic with an $L1_2$ structure, where the Ni atoms occupy the face centers and the Al atoms occupy the corners of the unit cell in the composition range of 25–27 at. % Al ($T\leqslant 400$ °C).[15] It is the γ' phase, in dispersed coherent precipitate form, that provides the superior strength observed in commercial superalloys, particularly at elevated temperatures.

Previous work by Eridon, Was, and Rehn[4] demonstrated the formation of a unique "dual-phase" structure in irradiated Ni-Al thin films. Multilayers with a composition in the range of Ni-(16-23 at. %) Al, were deposited onto polished Ni substrates and ion-beam mixed with 500-keV Kr. Irradiation resulted in an increase in grain size to about the thickness of the film (600 Å) and in the formation of a solid-solution γ phase. The microstructure was observed to possess a texture related to the orientation of the underlying, coarse-grained (>100 μm) Ni substrate. Annealing of this ion-beam-mixed structure at 425 °C for 1 h resulted in the transformation to $\gamma+\gamma'$ phases, but the morphology was such that distinct, coarse grains ($\geqslant 600$ Å-diam) of both phases were observed (dual-phase microstructure). Furthermore, the γ' grains formed with the same texture observed in the γ phase following irradiation. Assuming that the irradiated film consisted of initially homogeneous grains, substantial lattice diffusion was required to permit the composition changes necessary for the formation of the equilibrium phases in the dual-phase morphology. It was puzzling how such compositional changes could occur given the large irradiated grain size and the relatively small thermal diffusion distances (<60 Å) characteristic of the annealing conditions used.

The present study sought to further understand phase formation in ion-irradiated and annealed Ni-Al multilayers. In order to accomplish this, irradiation and annealing studies were conducted on transmission electron micros-

[a]Present address: Argonne National Laboratory, MSD-212, 9700 S. Cass Ave., Argonne, IL 60439.

 0021-8979/91/042021-08$03.00 © 1991 American Institute of Physics

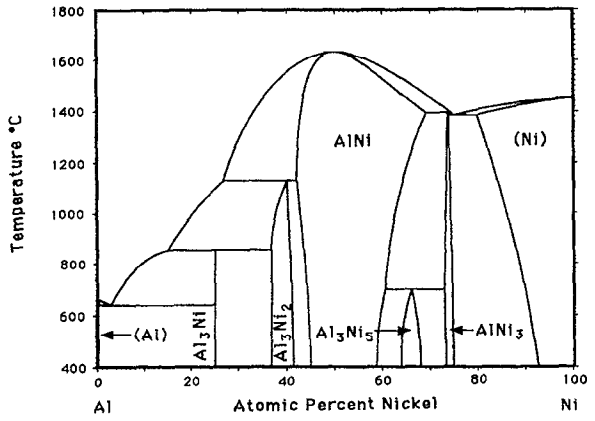

FIG. 1. Binary phase diagram for Ni-Al from Ref. 15.

copy (TEM) grids supporting thin multilayer and coevaporated Ni-Al alloy films. Emphasis was placed on phase formation during post-irradiation annealing of mixed multilayers. The results indicated that the presence of Cu in the films, and irradiation-induced textures, significantly affected the resulting phase formation.

II. EXPERIMENT

Thin films of multilayer and coevaporated Ni-Al alloys with compositions in the range of 18–23 at. % Al were prepared by electron-beam evaporation at room temperature in an oil-less, cryopumped vacuum system in which the pressure was 9×10^{-7} Torr or less during deposition. The films used varied between 400 and 600 Å total thickness with deposition rates between 1 and 10 Å/s. Multilayer films were prepared by sequential evaporation of each alloying element without breaking vacuum. The relative thickness of the individual layers was controlled to yield the desired overall film composition. Typically, six Ni layers and five Al layers were used. For coevaporated films, simultaneous deposition from two separate sources was conducted with the relative deposition rate of the sources controlled to yield the desired film composition.

Films were deposited onto polished Si pieces as well as 3-mm-diam TEM grids (Cu, Ni, or Mo) embedded in an amorphous Crystalbond substrate on a glass microscope slide. After the evaporation, the grids were removed from the glass slide by dissolving the Crystalbond in acetone, allowing the films to span holes of the grids.

The thickness and composition of the films deposited onto Si were examined using Rutherford backscattering spectrometry (RBS). RBS was performed using 2-MeV He ions on a tandem accelerator at the Michigan Ion Beam Laboratory for Surface Modification and Analysis (MIBL).[16] Raw data were analyzed using the RUMP analysis code.[17] Composition analysis was also performed using x-ray energy dispersive spectroscopy (XEDS) in a JEOL 2000FX analytical transmission electron microscope.

Room-temperature irradiations were conducted using ion beams available at both the MIBL and the High Voltage Electron Microscopy (HVEM) facility in the Materials Science Division at Argonne National Laboratory (ANL).[18] A 400-kV Varian Extrion implanter in the MIBL was used to produce beams of 700-keV Xe and 80-keV Cu. At ANL the HVEM was interfaced with a beamline from a tandem accelerator and *in situ* irradiations were performed using 1.7-MeV Xe ions. At both energies of Xe used for irradiations, the range R_p minus the straggling ΔR_p of the ions, as determined by TRIM-89 calculations,[19] was substantially beyond the film thickness and thus avoided significant deposition of Xe in the films (700-keV Xe: 930±300 Å; 1.7-MeV Xe: 2150±590 Å). The energy of the Cu ions was chosen to center the implant profile within the alloy film (80-keV Cu: 250±120 Å). The vacuum in the end station was typically in the $(7–9) \times 10^{-7}$ Torr range during irradiation. Ion-beam power inputs were maintained below 0.25 W/cm^2 to minimize beam-induced heating. Ion doses sufficient to homogenize the multilayers were used and were typically $\geqslant 7.5 \times 10^{15}$ cm^{-2} for the Xe ions. Irradiation with Cu caused simultaneous mixing and alloying of multilayer films. In order to homogenize the films, a dose of 1.5×10^{16} cm^{-2} was used to match the damage induced by the Xe irradiations, resulting in a peak concentration of 6 at. % Cu.

Following irradiation, anneals were conducted on a number of the alloy films in order to observe the phase transformations. The anneals were isothermal, and performed at varying times and temperatures. The two techniques used were vacuum annealing *in situ* in the electron microscope and annealing in a purified Ar flow furnace; both provided identical results.

Transmission electron microscopy was used to analyze the microstructure and phases present in films after the treatments described above. Detection of the γ' phase in the films was readily accomplished using electron diffraction in TEM. The ordered structure of the γ' phase gives rise to diffraction rings normally absent in FCC structures, and hence its presence is easily confirmed (see Fig. 2). These reflections were used to perform dark-field imaging to examine the morphology of the γ' phase. Composition analysis of both post-annealed and post-irradiated films was conducted using XEDS in TEM.

III. RESULTS

A. Effects of irradiation

Both multilayer and coevaporated films consisted of metastable, solid-solution gamma (γ), and hexagonal close-packed (HCP) phases following irradiation with Xe to doses $\geqslant 7.5 \times 10^{15}$ cm^{-2}. The HCP phase was not observed in samples irradiated with Cu for doses up to 1.5×10^{16} cm^{-2}. The HCP phase was observed to form at a substantially lower dose in the irradiated multilayers (5×10^{14} cm^{-2}) than in the coevaporated films (5×10^{15} cm^{-2}).

Figure 3 shows selected-area electron-diffraction patterns (SADPs) at varying tilts in TEM for coevaporated and multilayer films after irradiation with 1.7-MeV Xe in the HVEM. In the coevaporated film [Fig. 3(a)], all ring

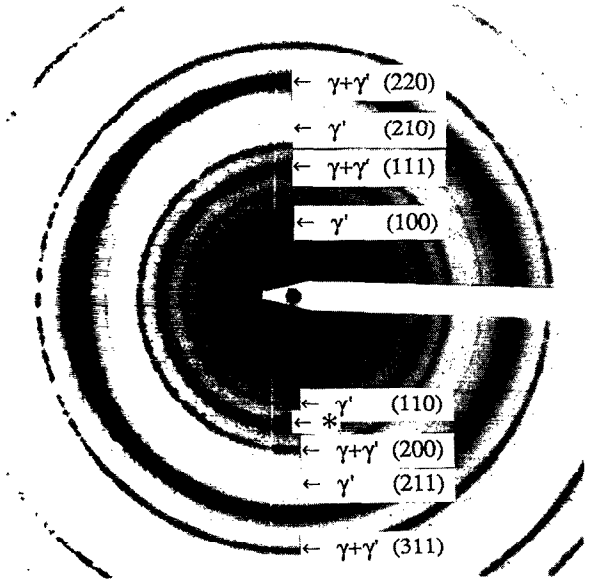

FIG. 2. Selected-area electron-diffraction patterns from a Ni-20 at. % Al multilayer film annealed at 450 °C for 1 h. The presence of an ordered γ' phase is indicated by the normally absent FCC rings. The ring identified with an asterisk is due to twinning and double diffraction.

reflections from both the γ and HCP phases were observed. Several reflections from both phases were missing in the pattern for the multilayer sample shown in Fig. 3(c). Their absence was indicative of strong textures present in the multilayer film which are discussed further below. Analysis of the HCP reflections indicated that the HCP phase had lattice parameters of $a = 2.6$ Å and $c = 4.1$ Å. The morphology and grain size of the γ and HCP phases were observed to be similar at high doses. Furthermore, the similarity in lattice spacings between planes of the γ and HCP phases indicated that the two phases were quite similar structurally. They could be thought of as differing only in the stacking sequence of lattice planes.

Crystallographic textures were observed to form in both types of films as a result of irradiation. Strong textures occurred in both the γ and HCP phases in the ion-beam-mixed multilayers. This texture was illustrated by SADPs taken from a multilayer sample irradiated with 1.7-MeV Xe to 2.5×10^{16} cm^{-2}, which are shown in Figs. 3(c) and 3(d). Although this particular dose was high, the results were consistent with those obtained from other samples irradiated in the dose range of $(0.75\text{–}1.0)\times10^{16}$ cm^{-2}. The pattern in Fig. 3(c) was taken with the electron beam normal to the film, and the pattern in Fig. 3(d) was taken with the beam incident at about 45°. In the normal-incidence pattern, for the γ phase, only rings corresponding to ($hh0$), where $h=2n$ ($n=1,2,...$), appeared. In the same pattern, only ($hk0$) rings appeared for the HCP phase. The pattern was indicative of both a ⟨111⟩ γ phase texture and a ⟨001⟩ HCP texture. In both instances, the close-packed planes of each phase lie parallel to the film surface. When the sample was tilted in the microscope, as shown in Fig. 3(d), the missing reflections of each phase were observed. The observed textures formed even when the irradiation was performed with the ions incident at an $\sim16°$ angle with respect to the film normal.

Irradiation-induced texture was less pronounced in coevaporated alloy films and appeared restricted predominantly to the HCP phase. The texture in the coevaporated films is demonstrated by the SADPs shown in Figs. 3(a) and 3(b).

In addition to observations of phase formation and texture, irradiation also caused grain growth to occur in the alloy films. The amount of growth induced was found to be strongly dependent upon the initial structure of the films.[20] Ni-Al multilayers experienced significantly greater ion-induced grain growth than did coevaporated films of the same composition under the same irradiation conditions. For 700-keV Xe ions, multilayers grew from an as-evaporated grain size of $\leqslant$100 to 630 Å after a dose of 5×10^{15} cm^{-2}. During the same dose increment, the grain size of the coevaporated films increased from $\geqslant$100 to 360 Å. These observations prompted further study into ion-induced grain growth phenomena in which grain size as a function of ion dose was examined for a variety of multilayer and coevaporated alloy thin films.[21]

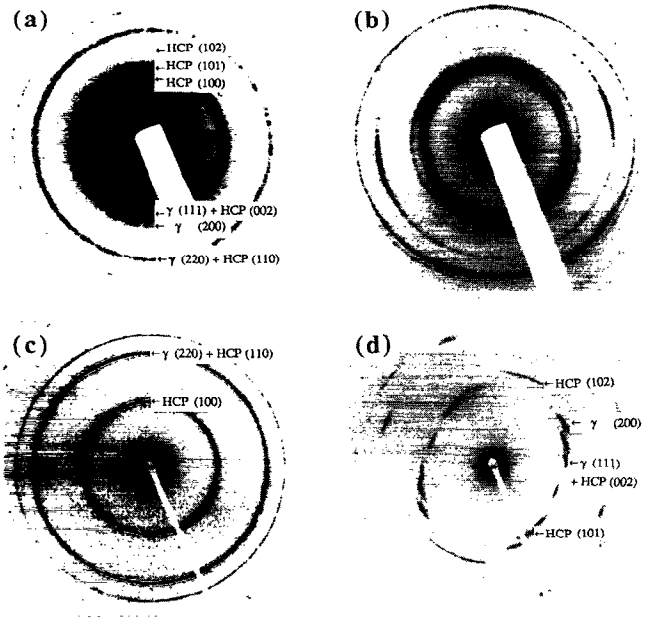

FIG. 3. Selected-area electron-diffraction patterns revealing phases and textures in Ni-20 at. % Al films irradiated with 1.7-MeV Xe. (a) and (b) Coevaporated film irradiated to 10^{16} cm^{-2} and examined at 0° and 45° tilts, respectively, in the TEM. (c) and (d) Multilayers irradiated to 2.5×10^{16} cm^{-2} and examined at 0° and 45° tilts, respectively, in the TEM.

B. Effects of post-irradiation annealing

Annealing of the irradiated multilayer films at 450 °C for 1 h resulted in the transformation from the metastable solid-solution γ and HCP phases to the $\gamma+\gamma'$ phases as predicted by the Ni-Al phase diagram (Fig. 1). The HCP phase transformed at a relatively low temperature,

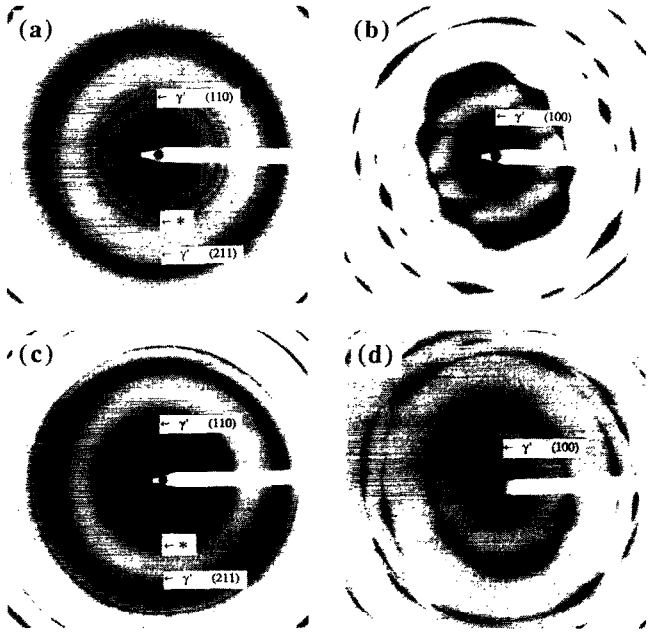

FIG. 4. Selected-area electron-diffraction patterns from Ni-20 at. % Al multilayers irradiated with 700-keV Xe to 7.5×10^{15} cm^{-2} and annealed at 450 °C for 1 h. (a) and (b) show a sample supported by a Cu TEM grid at 0° and 45° tilts, respectively. Sharp γ' rings were present. (c) and (d) show a sample supported by a Mo TEM grid at 0° and 45° tilts, respectively. Diffuse γ' rings were present. The ring with an asterisk is due to twinning and double diffraction.

$\sim$300 °C, as determined by the disappearance of the HCP rings from SADPs during the heater ramp-up in the TEM.

It was noted that in all the annealed multilayers, in addition to the $\gamma+\gamma'$ phases, SADPs showed the presence of a ring with an interplanar spacing of 2.17Å. This ring is indicated by an asterisk in Figs. 2, 4, and 8, and was suspected to originate from a combination of twinning and double diffraction similar to that observed previously for evaporated Au thin films with a ⟨111⟩ orientation.[22] This interpretation was supported by the fact that this isolated ring's interplanar spacing did not match with any of those of the Ni-Al alloys or common oxides (e.g., NiO, Al_2O_3). Furthermore, it could not be associated with the HCP phase, because this phase was absent subsequent to annealing.

The morphology of the γ' phase that developed in the annealed multilayers depended strongly on the type of TEM grid used to support the film during irradiation and annealing. Figure 4 shows a comparison between ion-mixed multilayers, annealed under the same conditions (450 °C, 1 h) on copper or molybdenum TEM grids. In the Cu grid sample [Figs. 4(a) and 4(b)], distinct γ' reflections were present after annealing, and the γ' phase had the same strong texture as the irradiated-only sample. In the Mo grid samples [Figs. 4(c) and Fig. 4(d)], only diffuse γ' rings were present after annealing, again with the same texture as the irradiated samples. The diffuse nature of the γ' rings in the Mo grid sample was indicative of very small precipitates. Results identical to the Mo grid results were obtained for films irradiated and annealed on Ni grids.

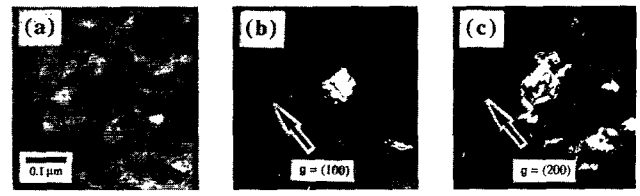

FIG. 5. TEM images of the microstructure of a Ni-Al multilayer sample on a Cu TEM grid irradiated with 700-keV Xe to 7.5×10^{15} cm^{-2} and annealed at 450 °C for 1 h demonstrating the dual-phase morphology. (a) Bright-field image, (b) and (c) dark-field images of the exact same area as in (a).

Figure 5 shows the dual-phase morphology of $\gamma+\gamma'$ typically observed in irradiated and annealed Ni-Al multilayers on Cu grids. This morphology was associated with the presence of the distinct, sharp γ' reflections as shown in Figs. 4(a) and 4(b). Furthermore, this morphology was restricted to regions in close proximity to large masses of Cu (e.g., grid bar). The sequence of TEM images demonstrated the coarse-grained nature of the γ' in which grain sizes were approximately the same as those observed in the γ phase ($\sim$700 Å). This morphology corresponds to the "dual-phase structure" observed in previous work.[4]

In order to isolate the effect of Cu on phase formation in irradiated and annealed multilayers, an implantation was performed using 80-keV Cu ions to both mix and alloy multilayers on Mo TEM grids. Following implantation to 1.5×10^{16} cm^{-2}, a strong ⟨111⟩ γ phase texture was present in the films, but the HCP phase, observed in Xe irradiations, was absent. XEDS determined that the film had a Cu content of $\sim$6 at. %. The dual-phase structure was observed to form as a result of annealing at 450 °C for 1 h. Figure 6 shows a bright-field/dark-field sequence illustrating the coarse-grained nature of the γ' phase. The microstructure was quite similar to that pictured in Fig. 5 and was uniform throughout the implanted film.

The quite different morphology of γ' observed in irradiated and annealed Ni-Al multilayers on Mo grids was demonstrated in the TEM images shown in Fig. 7. Unlike the Cu grid samples, imaging with a γ' ring showed very small ($\leqslant$50-Å-diam) precipitates within γ grains. The small size of these precipitates shown in Fig. 7(b) gave rise to the diffuse γ' rings observed in the SADPs obtained

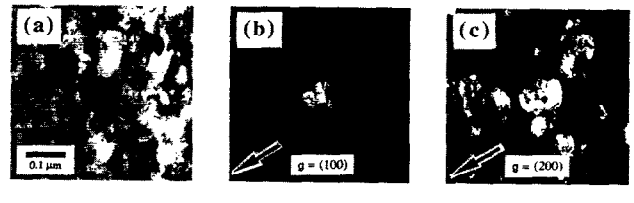

FIG. 6. TEM images of the microstructure of a Ni-Al multilayer sample on a Mo TEM grid irradiated with 80-keV Cu to 1.5×10^{16} cm^{-2} and annealed at 450 °C for 1 h demonstrating the dual-phase morphology. (a) Bright-field image, (b) and (c) dark-field images of the same area as in (a).

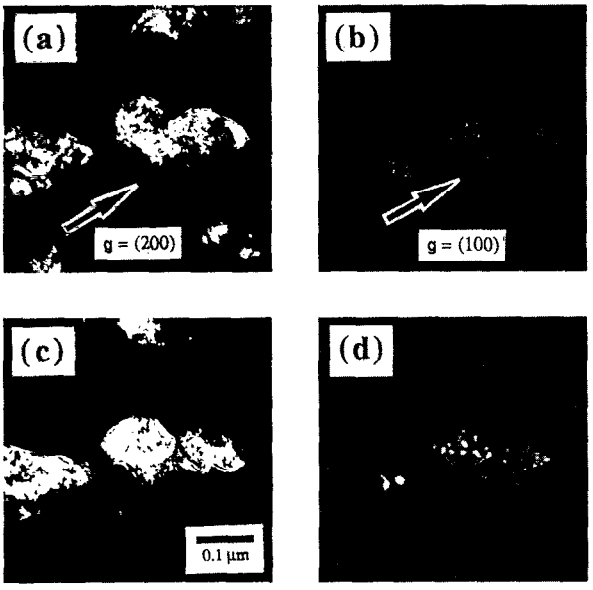

FIG. 7. Dark-field images of the microstructure of a Ni-Al multilayer sample on a Mo TEM grid irradiated with 700-keV Xe to 7.5×10^{15} cm^{-2} and annealed. (a) and (b) show the same area after annealing at 450 °C for 2 h and 550 °C for 1 h, imaged using the $\gamma+\gamma'$ (200) and the γ' (100) reflections, respectively. (c) and (d) show the same area, under the same imaging conditions, as in (a) and (b) following additional annealing at 700 °C for 1 h.

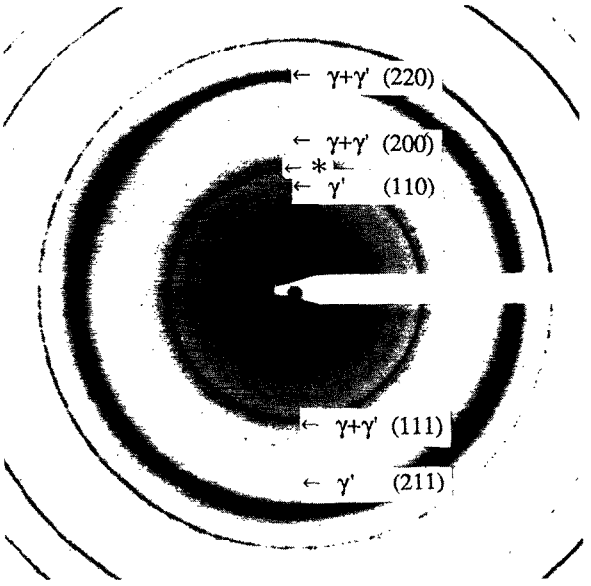

FIG. 8. Selected-area electron-diffraction pattern obtained from a Ni-Al multilayer sample, at 0° tilt, irradiated with 700-keV Xe to 5×10^{15} cm^{-2} and annealed at 450 °C for 1 h. The ring identified with an asterisk is due to twinning and double diffraction.

from these samples [Fig. 4(c) and (d)]. Upon further annealing at 700 °C for 1 h, Fig. 7(d) shows that the γ' precipitates grew into particles with a size on the order of 200 Å. The dark-field images of the $\gamma+\gamma'$ phases [Fig. 7(a) and (c)] showed that little, if any changes in the microstructure (e.g., grain growth) were observed even after annealing at 700 °C. The dark-field image in Fig 7(d) appeared to show the γ' forming preferentially along (100) matrix planes.

In irradiated multilayers, γ' appeared to form exclusively with a ⟨111⟩ fiber texture. This was demonstrated by the SADP shown in Fig. 8 obtained from an irradiated and annealed multilayer sample. This film was only irradiated to a dose of 5×10^{15} cm^{-2} and did not exhibit the complete texture observed in films irradiated to higher doses. The presence of the γ (111) and γ (200) reflections following irradiation was evidence of the incomplete texture. After annealing the film at 450 °C for 1 h, diffuse γ' reflections from the (110) and (211) planes were observed (see Fig. 8). The absence of other γ' reflections indicated that the γ' was forming with a ⟨111⟩ texture even though the microstructure still contained a number of randomly oriented grains.

IV. DISCUSSION

A. Effects of irradiation

Unique to the present study were observations of phase formation in irradiated Ni-rich, Ni-Al coevaporated films. The results, depicted in Figs. 3(a) and 3(b), showed that the same phases were present as in the multilayer films after irradiation to the highest doses. The coevaporated films were fabricated as supersaturated γ, and this phase remained throughout the irradiation. The HCP phase was also observed at the highest doses. Two major differences in phase formation and microstructure resulting from irradiation were noted between the coevaporated films and multilayers of similar composition. First, the HCP phase was observed to form at a larger dose (5×10^{15} cm^{-2}) than in the multilayer films (5×10^{14} cm^{-2}). Second, the strong texture present in ion-beam-mixed multilayers was much less pronounced in irradiated coevaporated films. Both of these differences may in part be attributed to the role that the thermochemical quantity, heat-of-mixing (ΔH_{mix}), has in multilayers, but not in coevaporated films. The release of ΔH_{mix} upon irradiation could have enhanced atomic mobility in the multilayers and speeded the kinetics of phase formation and texturing.

The HCP phase has been observed in a number of irradiation experiments involving both elemental Ni and Ni-Al thin films.[1,8,23–25] Hence, its formation is not limited to an alloying effect of Al. It has been postulated that the formation of HCP is a result of a martensitic transformation due to stresses induced by irradiation.[8,25] Also, the fact that the HCP phase formed in multilayers but not in γ' films irradiated at 80 K led Eridon and co-workers[1] to suggest that the heat-of-mixing released in the multilayers enhanced the kinetics of diffusion and permitted the HCP phase to form. In the latter case, a certain minimum irradiation dose, or displacements per atom (dpa), was required for the HCP phase to form. The results observed in the present work tend to support this atomic diffusion description. Under conditions where both the composition of the films and irradiation conditions were identical, as in the present study, the energy release due to ΔH_{mix} in the multilayers could have enhanced atomic mobility, achieving

the minimum atom rearrangements required for HCP formation at an earlier dose than in the coevaporated films.

In addition to the effect of enhanced atomic mobility, the earlier HCP formation in the multilayers may be attributed to local composition variations present during irradiation that are absent from the coevaporated films. Previous work examining Al^+ implantation in Ni observed that the HCP phase formed at Al compositions in the vicinity of 33 at. % Al.[8] During ion-beam-mixing, portions of the multilayers are expected to possess this composition at intermediate doses prior to homogenization. Because of this composition effect, the HCP phase could have nucleated in localized areas at doses lower than those required by displacements alone.

The second major difference in microstructure between the multilayers and coevaporated films was a variation in textures. The strong textures present in the irradiated multilayers, demonstrated in Figs. 3(c) and 3(d), formed with the close-packed γ and HCP planes parallel to the film surface. These textures were surface related and not the result of a channeling effect of the incident ions, as demonstrated by the fact that the HVEM irradiations, performed with the ion-beam incident at an angle ($\sim 16°$) to the film surface, resulted in the same textures as those caused by normal-incidence irradiation. Moderate-to-strong textures have been commonly observed in previous irradiation experiments involving metal films[26] and multilayers.[27–29] These textures have previously been attributed to a reduction in surface energy that accompanies the alignment of the close-packed atom planes with the film surface.

The present work suggests that the existence of the strong irradiation-induced textures in multilayers and their absence in coevaporated films was a combination of two factors. The first factor was the presence of slight $\langle 111 \rangle$ FCC textures in the as-evaporated multilayer films that were not present in the coevaporated films. The slight phase textures in the multilayers provided sites for nucleation of both the $\langle 111 \rangle$ γ phase and $\langle 001 \rangle$ HCP phase textures during irradiation. The second factor accounting for differences in texture is identical to the explanation of the HCP phase formation described above. The ΔH_{mix} released during irradiation of the multilayers enhanced atomic mobility, permitting the textures to form more readily than in the coevaporated films. This ΔH_{mix} effect was presumably not solely responsible for the observed texture since previous ion-beam-mixing studies have demonstrated strong textures in multilayers samples in which the heat-of-mixing is positive [e.g., Ag-Ni (Ref. 29)]. However, the added mobility due to this heat-of-mixing, combined with the presence of a slight texture prior to irradiation, resulted in a more pronounced irradiation-induced texture in the multilayers than in the coevaporated films.

B. Effects of post-irradiation annealing

Formation of the γ' in irradiated films on Mo and Ni TEM grids were observed to proceed via a traditional nucleation and growth mechanism.[30] The qualitative observations of the microstructure, as shown in Fig. 7, support this conventional growth description. Particle sizes, morphologies, and growth rates were observed to be similar to those reported for bulk, solution-treated alloys.[31–36] For example, Ardell and Nicholson[32] reported γ' precipitates with an average size of 190 Å following the anneal of a bulk supersaturated Ni-13 at. % Al alloy at 750 °C for 1 h. Furthermore, Fig. 7(d) shows that some of the larger γ' particles have flat edges parallel and perpendicular to the (100) reciprocal lattice vector. This indicated that the precipitates were forming coherently along (100) planes, as has also been observed in bulk experiments.[32]

The role that the strong irradiation-induced textures have in the subsequent phase formation in films on Mo and Ni TEM grids is unclear. All the films used on Mo and Ni grids showed the strong $\langle 111 \rangle$ γ texture that was not removed by annealing. However, whether these were necessary for the γ' formation is uncertain since no films were annealed without these textures being completely present in the microstructure of the films prior to the anneals. It appeared that in the case of films on Mo and Ni grids, the role of irradiation was simply to induce homogenization, thus forming a supersaturated alloy in a manner similar to conventional solution treating and quenching.

Discussion of the substantial effect of Cu in phase formation in the ion-beam-mixed films requires addressing both its potential thermodynamic and kinetic effects. Thermodynamically, no changes in phase formation are expected for substantial incorporation of Cu in the films. Cu has been observed to substitute readily for Ni in the γ' phase.[37–40] At 500 °C, the ternary phase diagram[41] indicates that additions of up to 25 at. % Cu will not change the phases ($\gamma + \gamma'$) present in the microstructure. However, the presence of Cu may well have promoted the incoherent nucleation of γ', the subsequent growth of which resulted in the dual-phase morphology.

It is also likely that the effect of Cu is a kinetic one, permitting more rapid nucleation and growth of γ' precipitates. Table I summarizes data for tracer lattice diffusion in Ni. While the diffusion in the nondilute ternary alloy is expected to be more complex, this data provides a basis upon which to make qualitative conclusions. Based on this data, diffusion distances were estimated for the solutes for an anneal performed at 450 °C for 1 h. The results indicate that Cu diffuses more readily than Ni in Ni, and so the kinetics of nucleation and growth should be quickened. Liu and Wagner[45] determined an activation energy of 50 kcal/mol for γ' coarsening in a Ni-36 at. % Cu-9 at. % Al alloy. This was lower than the 64 kcal/mol determined for coarsening in the Ni-Al system without Cu.[32] Both Liu and

TABLE I. Lattice diffusion data for Ni, Cu, and Al tracer diffusion in Ni. D_0 is the preexponential factor, Q is the activation energy, and $(4Dt)^{1/2}$ is the mean diffusion distance in time t. Compiled from Refs. 42–44.

Solute	D_0 (cm^2/s)	Q (eV)	$(4Dt)^{1/2}$ 450 °C, 1 h
Ni	0.92	2.88	1 Å
Cu	0.57	2.68	4 Å
Al	1.0	2.39	58 Å

Wagner's work[45] and a study examining aging of a Ni-Cu-Al commercial alloy[46] showed that γ' precipitates grew to larger sizes under similar annealing conditions than those growing in Ni-Al alloys.[31–36]

Having described the nucleation and kinetic effects expected by the presence of Cu in the irradiated multilayers, the task then becomes determining the mechanism of Cu incorporation into the film. The results of this work indicated that the dominant mechanism of Cu incorporation was diffusion during thermal annealing subsequent to ion-beam-mixing. More specifically, grain-boundary and surface diffusion were the likely sources. The strong $\langle 111 \rangle$ γ phase texture formed during ion-beam-mixing resulted in a preponderance of tilt boundaries between the columnar grains of the microstructure. These boundaries, in areas of the film located over the Cu grid, likely provided high-diffusivity paths for penetration of the Cu in the film.

Low-angle tilt boundaries may be modeled as a sequence of parallel-stacked, edge dislocations. The cores of these dislocations provide a free volume that allows more rapid diffusion parallel to these cores than in the lattice.[47,48] In this manner, dislocation pipe diffusion combined with the large amount of grain-boundary area due to the small grain size ($\sim$700 Å) could have permitted substantial diffusion of Cu into the textured film. The diffusion could continue, at a slower rate, in paths perpendicular to the dislocations along the boundaries, penetrating laterally into the film. This lateral diffusion was augmented by surface diffusion. Having saturated grain boundaries, the Cu could then diffuse into the volume of the grains, providing the composition change necessary to form the equilibrium γ' phase.

Coevaporated alloy films irradiated and annealed on Cu grids showed no evidence of dual-phase formation. This observation further attested to the important role that the irradiation-induced texture had in the transport of Cu into the multilayer films via grain-boundary diffusion. Surface diffusion of Cu was also observed in the coevaporated films, but the absence of texture presumably reduced the ability of Cu to diffuse into the film.

Based on the above discussion, it is concluded that the dual-phase formation in TEM-supported grid films was the result of an alloying effect of Cu in combination with a strong irradiation-induced texture. The textured microstructure permitted rapid diffusion into the ion-beam-mixed film upon annealing. In this respect phase formation was analogous to the dual-phase formation observed previously in films irradiated on Ni substrates.[4,49] In these earlier studies pronounced textures, related to the underlying Ni grains, were also observed.

V. CONCLUSIONS

Ion irradiation and annealing experiments were performed on multilayer and coevaporated Ni-Al alloy films of nominal composition Ni-20 at. % Al. The results supported the following conclusions.

Ion-beam-mixing of multilayers formed metastable, supersaturated γ, and HCP phases. Irradiation of coevaporated films resulted in these same phases.

The formation of pronounced textures ($\langle 111 \rangle$ γ and $\langle 001 \rangle$ HCP) in irradiated multilayers supported by TEM grids was attributed to the presence of a slight as-evaporated texture combined with the heat-of-mixing release in multilayers during irradiation. The heat-of-mixing effect, which was absent in coevaporated films, likely enhanced atomic mobility in the multilayers, permitting the textures to form more readily (e.g., at smaller ion doses). The textures formed with the close-packed planes parallel to the surface, consistent with the minimization of surface energy.

The formation of γ' in post-irradiation annealed multilayers which contained no Cu appeared to proceed by a traditional diffusional growth mechanism, resulting in small, coherent γ' precipitates in γ matrix grains.

The presence of Cu in ion-beam-mixed multilayers during post-irradiation annealing permitted the formation of a dual-phase $\gamma + \gamma'$ structure. The results suggested that Cu affected the nucleation of γ' precipitates, perhaps by creating incoherent interfaces, and increased the kinetics of growth, resulting in the coarse γ' morphology.

It is believed that the strong irradiation-induced texture assisted the formation of the dual-phase structure in multilayers irradiated and annealed on Cu TEM grids. The pronounced texture created numerous tilt boundaries perpendicular to the film surface, providing high-diffusivity paths for Cu to enter the film from the TEM grid during annealing.

ACKNOWLEDGMENTS

The authors gratefully acknowledge the use of facilities and assistance provided by the following: Michigan Ion Beam Laboratory for Surface Modification and Analysis (A. Mashayekhi and V. Rotberg) and Electron Microscopy and Analysis Laboratory (J. Mansfield), both at the University of Michigan, High Voltage Electron Microscope-Tandem Facility (L. Funk, S. Ockers, and E. Ryan) at ANL, and HB 501 STEM (R. Casper and T. Kelly) at the University of Wisconsin. This work was funded under NSF Grant Nos. DMR8603174 and DMR8903138 (D. Alexander and G. Was) and DOE Contract No. W-31-109-ENG-38 (L. Rehn).

[1] J. M. Eridon, G. S. Was and L. E. Rehn, J. Mater. Res. **3**, 626 (1988).
[2] M. Ahmed and D. I. Potter, Acta Metall. **35**, 2341 (1987).
[3] M. Ahmed and D. I. Potter, Mater. Sci. Eng. **90**, 127 (1987).
[4] J. M. Eridon, G. S. Was, and L. E. Rehn, J. Appl. Phys. **62**, 2145 (1987).
[5] C. Jaouen, J. P. Riviere, and J. Delafond, Nucl. Instrum. Methods B **19/20**, 549 (1987).
[6] M. Nastasi, J. M. Williams, E. A. Kenik, and J. W. Mayer, Nucl. Instrum. Methods B **19/20**, 543 (1987).
[7] G. S. Was and J. M. Eridon, Nucl. Instrum. Methods B **24/25**, 557 (1987).
[8] M. Ahmed and D. I. Potter, Acta Metall. **33**, 2221 (1985).
[9] C. Jaouen, J. P. Riviere, A. Bellara, and J. Delafond, Nucl. Instrum. Methods B **7/8**, 591 (1985).
[10] D. I. Potter, M. Ahmed, and S. Lamond, in *Ion-beam Processing and Ion Implantation of Materials*, edited by G. K. Hubler, O. W. Holland, C. R. Clayton, and C. W. White (Materials Research Society, Pittsburgh, PA, 1984), pp. 117–126.

[11] L. S. Hung, M. Nastasi, J. Gyulai, and J. W. Mayer, Appl. Phys. Lett. **42**, 672 (1983).
[12] M. Nastasi, L. S. Hung, and J. W. Mayer, Appl. Phys. Lett. **43**, 831 (1983).
[13] D. J. Morrison, J. W. Jones, D. E. Alexander, C. Kovach, and G. S. Was, Mater. Sci. Eng. A **115**, 315 (1989).
[14] *The Superalloys*, edited by C. T. Sims and W. C. Hagel (Wiley, New York, 1972).
[15] *Binary Alloy Phase Diagrams*, edited by T. B. Massalski, J. L. Murray, L. H. Bennett, and H. Baker (American Society for Metals, Metals Park, OH, 1986).
[16] G. S. Was and V. H. Rotberg, Nucl. Instrum. Methods B **40/41**, 722 (1989).
[17] L. R. Doolittle, Nucl. Instrum. Methods B **9**, 334 (1985).
[18] C. W. Allen, L. L. Funk, E. A. Ryan, and A. Taylor, Nucl. Instrum. Methods B **40/41**, 553 (1989).
[19] J. P. Biersack and L. G. Haggmark, Nucl. Instrum. Methods **174**, 257 (1980).
[20] D. E. Alexander, G. S. Was, and L. E. Rehn, in *Beam-Solid Interactions: Physical Phenomena*, edited by J. A. Knapp, P. Borgesen, and R. A. Zuhr (Materials Research Society, Pittsburgh, PA, 1990), pp. 155–160.
[21] D. E. Alexander, G. S. Was, and L. E. Rehn, J. Appl. Phys. (submitted).
[22] P. Hirsch, A. H. Howie, R. B. Nicholson, D. W. Pashley, and M. J. Whelan, *Electron Microscopy of Thin Crystals* (Krieger, Malabar, FL, 1977), pp. 305–307.
[23] V. N. Bykov, V. A. Troyan, G. G. Zdorovtseva, and V. S. Khaimovich, Phys. Status Solidi A **32**, 53 (1975).
[24] I. Teodorescu and A. Glodeanu, Phys. Rev. Lett. **4**, 231 (1960).
[25] E. Johnson, T. Wohlenberg, and W. A. Grant, Phase Transit. **1**, 23 (1979).
[26] J. C. Liu, L. Jian, J. W. Mayer, C. W. Allen, and L. E. Rehn, in *Processing and Characterization of Materials Using Ion-Beams*, edited by L. E. Rehn, J. Greene, and F. A. Smidt (Materials Research Society, Pittsburgh, PA, 1989), pp. 297–302.
[27] B. Y. Tsaur, S. S. Lau, and J. W. Mayer, Appl. Phys. Lett. **36**, 823 (1980).
[28] B. Y. Tsaur, S. S. Lau, and J. W. Mayer, Philos. Mag. A **44**, 95 (1981).
[29] B. Y. Tsaur, and J. W. Mayer, Appl. Phys. Lett. **37**, 389 (1980).
[30] P. Haasen, Metall. Trans. A **16**, 1173 (1985).
[31] A. J. Ardell, Acta Metall. **16**, 511 (1968).
[32] A. J. Ardell and R. B. Nicholson, J. Phys. Chem. Solids **27**, 1793 (1966).
[33] A. J. Ardell and R. B. Nicholson, Acta Metall. **14**, 1295 (1966).
[34] S. Chambreland, A. Walder, and D. Blavette, Acta Metall. **36**, 3205 (1988).
[35] B. Reppich and G. Schumann, Mater. Sci. Eng. A **101**, 171 (1988).
[36] T. Suzuki, A. Tachikake, Y. Miyagawa, Y. Nishi, and E. Yajima, J. Phys. (Paris) Suppl. **47**, 221 (1986).
[37] R. W. Guard and J. H. Westbrook, Trans. Metall. Soc. AIME **215**, 807 (1959).
[38] A. K. Jena and M. C. Chaturvedi, J. Mater. Sci. **19**, 3121 (1984).
[39] W. O. Alexander, J. Inst. Met. **63**, 163 (1938).
[40] S. Ochiai, Y. Oya, and T. Suzuki, Acta Metall. **32**, 289 (1984).
[41] L. A. Willey, in *Metals Handbook: Metallography, Structures and Phase Diagrams*, edited by L. Taylor (American Society for Metals, Metals Park, OH, 1973), pp. 388–389.
[42] D. Gupta, in *Diffusion Phenomena in Thin Films and Microelectronic Materials*, edited by D. Gupta and P. S. Ho (Noyes, Park Ridge, NJ, 1988), pp. 1–72.
[43] W. Gust, M. B. Hintz, A. Lodding, H. Odelius, and B. Predel, Phys. Status Solidi A **64**, 187 (1981).
[44] D. Liu, W. A. Miller, and K. T. Aust, Acta Metall. **37**, 3367 (1989).
[45] Z. G. Liu and R. Wagner, J. Phys. (Paris) Suppl. **45**, 441 (1984).
[46] G. J. Marshall, Met. Sci. **18**, 553 (1984).
[47] P. S. Shewmon, *Diffusion in Solids* (The Minerals, Metals & Materials Society, Warrendale, PA, 1989).
[48] P. H. Pumphrey, in *Grain Boundary Structure and Properties*, edited by G. A. Chadwick and D. A. Smith (Academic, New York, 1976), pp. 139–200.
[49] D. E. Alexander, G. S. Was, and J. M. Eridon, Nucl. Instrum. Methods B **39**, 130 (1989).